ACS APPLIED MATERIALS & INTERFACES

Research Article

www.acsami.org

Optical Phenomena and Antifrosting Property on Biomimetics Slippery Fluid-Infused Antireflective Films via Layer-by-Layer Comparison with Superhydrophobic and Antireflective Films

Kengo Manabe, Shingo Nishizawa, Kyu-Hong Kyung, and Seimei Shiratori*

Department of Applied Physics and Physico-Informatics, Faculty of Science and Technology, Keio University, 3-14-1 Hiyoshi, Kohoku-ku, Yokohama, Kanagawa 223-8522, Japan

Supporting Information

ABSTRACT: Sophisticated material interfaces generated by natural life forms such as lotus leaves and *Nepenthes* pitcher plants have exceptional abilities to resolve challenges in wide areas of industry and medicine. The nano- and microstructures inspired by these natural materials can repel various liquids and form self-cleaning coatings. In particular, slippery liquid-infused surfaces are receiving remarkable interest as transparent, nonfouling, and antifrosting synthetic surfaces for solar cells and optical devices. Here we focus on the transparency of lubricant-infused texture on antireflective films fabricated by layer-by-layer self-assembly that decrease light scattering, which is important to maintain device properties. A slippery fluid-infused antireflective film composed of chitin nanofibers less than 50 nm in diameter prevented light scattering at the long-wavelength side by Rayleigh scattering to achieve 97.2% transmittance. Moreover, films composed of the same materials demonstrated three different morphologies: superhydrophilicity with antireflection, superhydrophobicity, and omniphobicity, mimicking the biological structures of moth eyes, lotus leaves, and pitcher plants, respectively. The effect of thermal changes on the ability of each film to prevent frost formation was investigated. The slippery fluid-infused antireflective film showed effective antifrosting behavior.

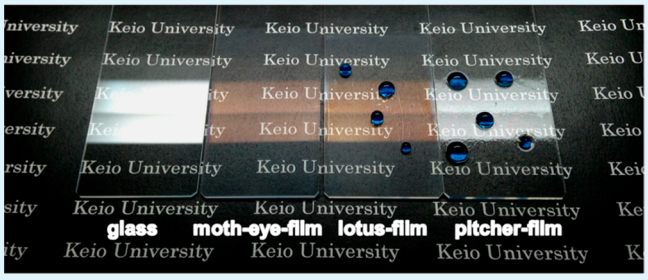

KEYWORDS: *superoleophobic surfaces, layer-by-layer, antireflective film, biomimetics, surface wettability, thermal change, antifrosting*

INTRODUCTION

Bioinspired materials are of interest for solving a wide variety of problems in broad-ranging areas from energy and the environment to biomedical devices.[1−3] With increasing emphasis on such materials, particularly controlled interfaces, micro/nanoarchitectures have emerged as a constantly advancing field. Excellent examples of innovative design concepts derived from natural life forms are the self-cleaning ability of lotus leaves,[4−6] antifouling effect of sharkskin,[7,8] antireflection of moth eyes,[9−11] water collection of the Namib Desert beetle,[12,13] and sticky surface of geckoes.[14,15] Among these examples, studies mimicking the self-cleaning of the lotus have greatly influenced interface science during the past decade.[16] The synthetic liquid-repellent surfaces based on this effect generate solid−air/liquid composite interfaces with low surface energy in composite micro/nanostructures, which maintain a high contact angle and a low contact angle hysteresis against water droplets or specific organic liquids.[17] Despite considerable effort, however, it remains difficult to produce surfaces that combine all of the following functions: repel low-surface-tension liquid,[18] tolerate scratches,[19] and possess high transmittance.[20] Additionally, transparent superhydrophobic films that tolerate subzero temperature variation are needed because there are few reports of superhydrophobic surfaces effective for antifogging, antifrosting, and removing frost.[21,22]

To overcome this shortcoming, Aizenberg et al.[23−26] offered convincing answers inspired by *Nepenthes* pitcher plants. They reported a strategy to produce self-healing slippery liquid-infused porous surfaces (SLIPSs) that outperform their natural counterparts and state-of-the-art synthetic liquid-repellent surfaces with their ability to repel various simple and complex liquids such as water and blood, maintain low contact angle hysteresis, and also exhibit antifrosting[22] and anti-icing[27] performance. Nano/microstructured substrates are used to lock an infused lubricating fluid in place. A structure with a low surface energy is necessary as an underlayer for the lubricant, on which the lubricant forms a stable, defect-free, and inert slippery interface (Figure 1S, Supporting Information).[28] Another related work indicated the transmittance change of SLIPSs.[29] By filling a porous film with lubricant, transmission increases because reflectance at the solid−gas interface and scattering by the nano/microstructure decrease. The above studies suggest that SLIPSs have the potential to exhibit high

Received: May 28, 2014
Accepted: August 5, 2014
Published: August 5, 2014

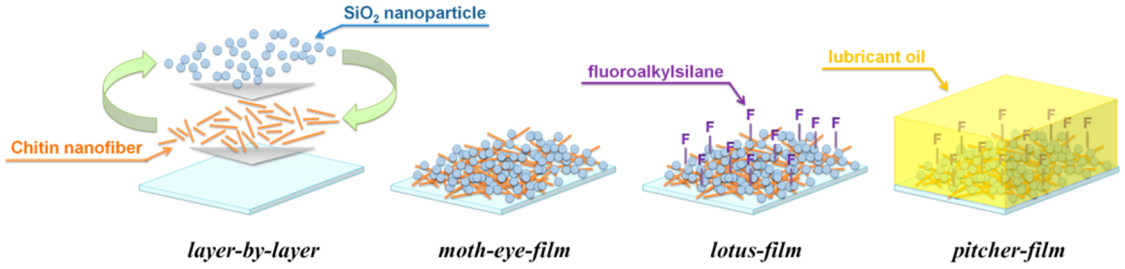

Figure 1. Schematic diagrams of the three phases of films. The antireflective moth-eye films consisted of chitin nanofibers (CHINFs) and silica nanoparticles (SiO_2) by layer-by-layer assembly. A superhydrophobic lotus film and lubricant-infused pitcher film were produced by functionalizing 10-bilayer moth-eye films.

transmittance if the underlayer for the lubricant is a superhydrophobic film with high transmittance and low reflectance. A slippery fluid-infused film that has the qualities of high transparency, antifouling ability, and adjustment to temperature change is expected to find application in solar panels and intelligent windows.

The idea to achieve such films was conceived from moth eyes, which have a graded refractive index and relief structures to decrease reflection.[30] Multilayer thin films mimic moth-eye structures that have been fabricated by layer-by-layer (LbL) assembly.[31] LbL assembly involves the alternate adsorption of oppositely charged materials by electrostatic attraction.[32−35] It is an easy, versatile, and convenient method that is performed at ambient temperature and pressure.[36−38] In addition, LbL assembly allows the surface texture, surface wettability, and thickness of a film to be controlled on the micro- and nanoscales. LbL films containing nanofibers or nanoparticles can possess a low refractive index and high porosity.[39−42] Films produced using this method have been developed for various applications such as antireflective,[43] superhydrophobic,[44] and omniphobic[45] coatings that mimic moth eyes, lotus leaves, and nepenthes (pitcher plant), respectively. SLIPSs with higher transmittance than 95% fabricated by a wet process have not been reported.[24−26] Indeed, although we reported gel-SLIPSs fabricated by a facile nanoscale phase separation method,[46] we were unable to achieve high transmittance using this method because it was difficult to control the surface roughness, film thickness, and optical properties. Therefore, using the LbL process to produce SLIPSs with high transparency and other various features such as stimulus responsivity[47−49] is an attractive possibility. In particular, antifrosting films, whose reflectance responds to fluctuation of the density of the liquid surface, intrinsically require antireflectivity because frosting is caused by the difference in temperature between opposite sides of glass windows and lenses, especially car windows. In some countries, frost formation on the car window has been a problem for a while now, and at the same time, it requires easily removing frost after increasing the temperature inside the car.

Here we report superhydrophilic and antireflective films (referred to as *moth-eye films*) composed of chitin nanofibers (CHINFs) and silica nanoparticles (SiO_2) formed by LbL assembly, a transparent superhydrophobic film (called the *lotus film*) that is a 10-bilayer *moth-eye film* hydrophobized by fluoroalkylsilane, and a slippery fluid-infused antireflective film (called the *pitcher film*) that is the *lotus film* covered by lubricant oil, as shown in Figures 1 and 2. This three-phase mimesis achieves an omniphobic coating with higher transmittance than previous research. Moreover, we reveal the antifrosting mechanism of the pitcher film by comparing the

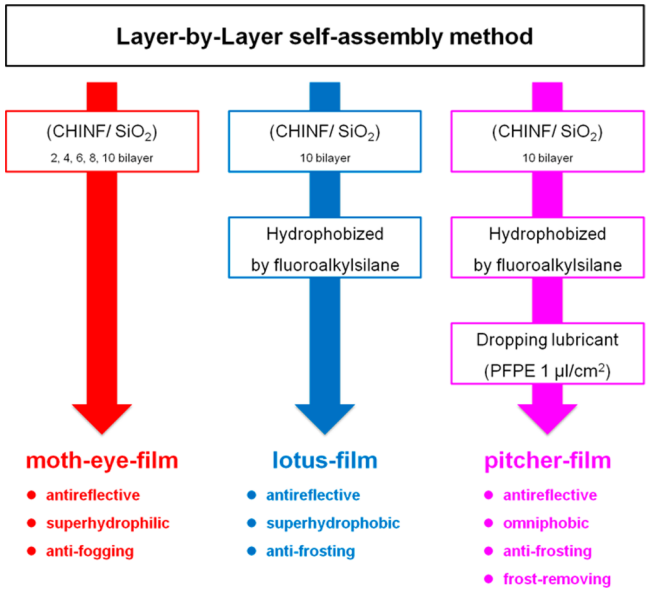

Figure 2. Outline of the experimental procedures and the properties of each type of film.

thermal changes of films with three kinds of surface wettability. Although the antifrosting ability of films with various kinds of surface wettability should consist of the same materials to allow comparison, a superhydrophilic film, superhydrophobic film, and liquid-infused film have not been directly compared, which allows the effect that lubricant oil has on the films to be revealed through this study.

EXPERIMENTAL SECTION

Materials. Crab shells (Kawai Hiryo, Iwata, Japan), colloidal silica nanoparticles (SiO_2; $\varphi \approx 30$ nm, Nissan Chemical Industries, Ltd., Japan), perfluoropolyether (PFPE) (Krytox GPL 103, $\gamma = 17.4$ mN m^{-1}, Dupont, United States), [5,5,6,6,7,7,8,8,9,9,10,10,10-trideca-fluoro-2-(tridecafluorohexyl)decyl]trichlorosilane (Gelest, Inc., United States), and glass substrates (76 × 26 mm, thickness 1.0 mm, refractive index 1.52, Matsunami Glass Industries, Ltd., Kishiwada, Japan) were used to produce the films. All LbL dipping suspensions were fabricated using ultrapure water (Aquarius GS-500.CPW, Advantec, Japan), and the suspension pH was adjusted using CH_3COOH (Kanto Chemical Co., Inc., Tokyo, Japan). The glass substrates were cleaned in KOH solution (1 wt % KOH/120 wt % H_2O/60 wt % IPA) for 2 min and then rinsed thoroughly with ultrapure water before use.

Refinement of Chitin Nanofibers. CHINFs were fabricated using the following method. The crab shells were first purified according to methods described in the literature.[50,51] First, crab shell powder was treated in 2 M HCl (Kanto) for 2 days at room temperature to remove mineral salts. After thorough rinsing with distilled water, the treated chitin powder was heated under reflux in 2

M NaOH (Kanto) for 2 days to remove protein. Next the pigment in the sample was removed using 1.7 wt % $NaClO_2$ (Kanto) in buffer solution for 6 h at 80 °C. After the sample was rinsed thoroughly with distilled water, it was suspended in 33 wt % NaOH containing $NaBH_4$ (0.03 g, Kanto), as described in a previous study.[52] The suspension including CHINFs, NaOH, and $NaBH_4$ was washed by pure water several times via centrifugation (5000 rpm, 5 min). Then the CHINF suspension was diluted to a concentration of 0.025 wt % and dispersed by ultrasonic wave.

Superhydrophilic and Antireflective Films (Moth-Eye Films). Superhydrophilic, antireflective, and low refractive index layers were fabricated with suspensions of refined CHINFs and SiO_2 by the LbL method. A glass substrate was alternately immersed in CHINF cationic suspension (0.025 wt %, pH 3) and SiO_2 anionic suspension (0.03 wt %, pH 3) for 1 min, rinsed with pure water for 3 min, and air-dried at a distance of 10 mm and force of 0.05 MPa after the deposition of each layer. The films covered about two-thirds of each glass substrate; about one-third was bare glass.

Transparent Superhydrophobic Film (Lotus Film). Transparent superhydrophobic layers were fabricated by the gas-phase method. A 10-bilayer CHINF/SiO_2 antireflective film was placed in a 100 mL plastic bottle along with a 2 mL glass bottle containing [6,6,7,7,8,8,9,9,10,10,10-tridecafluoro-2-(tridecafluorohexyl)decyl]-trichlorosilane (200 μL). The system was placed in thermal treatment equipment for 2.5 h at 70 °C.

Slippery Fluid-Infused Antireflective Film (Pitcher Film). PFPE (1 μL cm^{-2}) was added dropwise onto a lotus film. The PFPE layer was about 1 μm thick. Excess PFPE on the films was removed with a nitrogen gas flow.

Characterization. Field emission scanning electron microscopy (FE-SEM) and energy-dispersive X-ray spectrometry (EDX) images were taken using FE-SEM and EDX (S-4700, Hitachi, Japan) instruments with an accelerating voltage of 3 kV to characterize the surface morphologies of the films. Transmittance measurements in the spectral range of 300−1000 nm were carried out using a spectrophotometer (UVmini-1240, Shimadzu, Kyoto, Japan). The roughness of the films was analyzed by atomic force microscopy (AFM; Nanoscope IIIa, Digital Instruments, United States). The film thickness and refractive index of the ultrathin films coated on the glass substrate were determined by ellipsometry (MARY-102, Five Lab, Japan). Contact and sliding angles were measured using a contact angle meter (CA-DT, Kyowa, Japan). Total transmittance (TT), parallel transmittance (PT), diffusion (DIF), and haze (HAZE) values of the films were measured by a haze meter (NDH-5000, Nippon Denshoku Industries, Tokyo, Japan) with a white-light-emitting diode (5 V, 3 W) as an optical source.

Antifrosting Property Test. A glass substrate, moth-eye film (10-bilayer), lotus film, and pitcher film were set on a Peltier cooling unit in a thermohygrostat set at 10 °C and 80% relative humidity (RH), and then the Peltier unit was gradually cooled from +10 to −10 °C. Photographic images were recorded by a digital camera, and temperature changes were detected by thermography (PI400, Optris, United States). After all films were frosted, the unit was heated to 30 °C to compare frost removal ability.

RESULTS AND DISCUSSION

According to the Fresnel equations,[53] for an ideal homogeneous single-layer antireflective coating to have a reflective index of zero, the refractive index of the film on the glass substrate should be

$$n_l = \sqrt{n_{air} n_{substrate}} = \sqrt{1.52} \approx 1.23 \quad (1)$$

where n_l, n_{air}, and $n_{substrate}$ are the refractive indices of the low-refractive-index film, air, and substrate, respectively. Especially, in the case of vertical incidence, if the thickness of the medium equals one-quarter of the wavelength through it, surface reflectance would be 0% and light of that wavelength would transmit.[53] The refractive index of an LbL film can be estimated by a simple mixing rule:[54]

$$n_l = f_{air} n_{air} + f_{nanoparticle} n_{nanoparticle} + f_{polyelectrolyte} n_{polyelectrolyte} \quad (2)$$

where f_x and n_x are the volume fraction and refractive index of component x, respectively. According to this equation, porosity must be increased to decrease the refractive index of LbL films.

Also, a superhydrophobic film requires a relief structure and low surface energy.[55] The relief structure normally consists of a nano/micro complex surface, the high surface roughness of which causes transmittance to decrease by increasing scattering, as predicted by the optical theory for multilayer coatings:[56−60]

$$\ln(T/T_0) = -\{2\pi(n_{air} - n_l)\cos\theta\}^2(\sigma/\lambda)^2 \quad (3)$$

where T and T_0 are the transmittances of the multilayer with and without surface roughness, respectively, cos θ is the optical incidence angle to the outermost surface layer, σ is the RMS surface roughness, and λ is the wavelength. According to this equation, the RMS surface roughness is σ = 54.45 nm if each variable is set as follows: T/T_0 = 0.98, $\sigma/(\lambda \times 10^{-3})$, λ = 550 nm, and θ = 0. Therefore, the RMS surface roughness needs to be less than 54.45 nm to achieve high transmittance (more than 98%) and curb the decrease of transmittance due to scattering loss.

For the above-mentioned reasons, the films in this research need to achieve a refractive index of 1.23 in the superhydrophobic film (lotus film) and have low enough surface roughness to show a contact angle of 150°.

Superhydrophilic and Antireflective Films (Moth-Eye Films). First, superhydrophilic and antireflective films (moth-eye films) were fabricated by LbL assembly. As the number of bilayers increased, the film thickness increased linearly and the refractive index decreased (Figure 3). The lowest refractive index of the moth-eye film was 1.20. The film structures were porous and mainly consisted of particles (Figure 4A) because of the minimal electrostatic assistance of the CHINFs (Figure 2S, Supporting Information). The diameter of each CHINF was almost the same as the size of the nanoparticles (less than 50 nm), which prevented light scattering on the long-wavelength side by Rayleigh scattering.[53] With increasing thickness of the film structure, the surface roughness expressed as RMS (Rq) and Ra increased (Figure 4C).

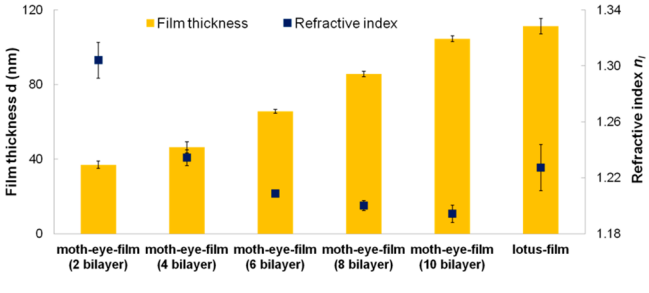

Figure 3. Film thickness (yellow bars) and refractive index (blue squares) of moth-eye films with different numbers of bilayers and the lotus film measured by ellipsometry.

The highest transmittance of the moth-eye film was 96.7% at 726 nm for 10 bilayers (Figure 5). This is because reflectance decreased because of the gradual increase of refractive index

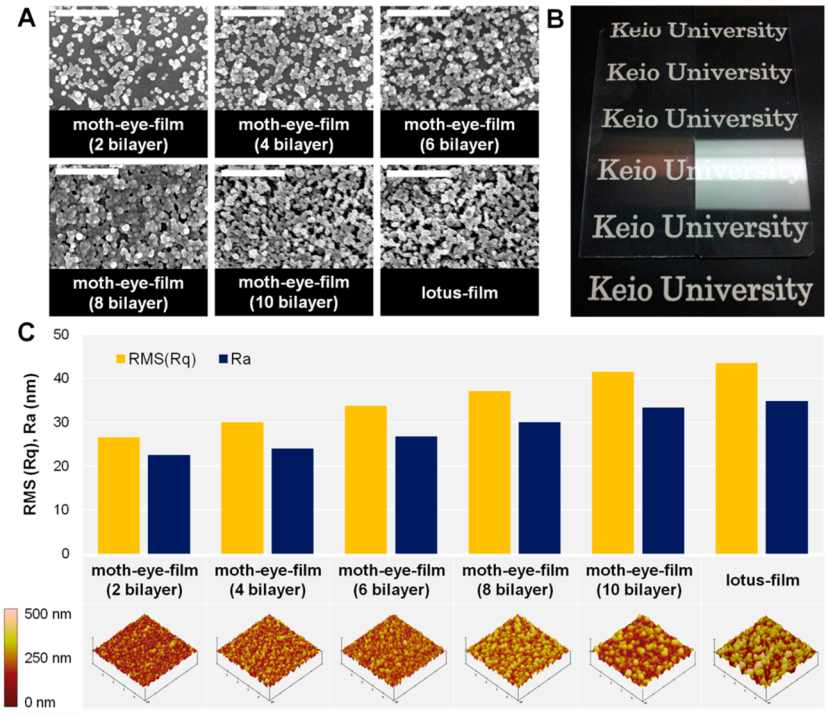

Figure 4. (A) FE-SEM images of moth-eye films with different numbers of bilayers and the lotus film. All scale bars are 1 μm. (B) Photographs of the moth-eye film (10-bilayer) (left) and glass substrate (right) under a fluorescent light. (C) Surface roughness determined by the RMS (Rq) (yellow bars) and Ra (blue bars) of moth-eye films with different numbers of bilayers and the lotus film, with corresponding AFM images shown below. The scan size (x and y) is 5 μm, and the data scale (z) is 500 nm.

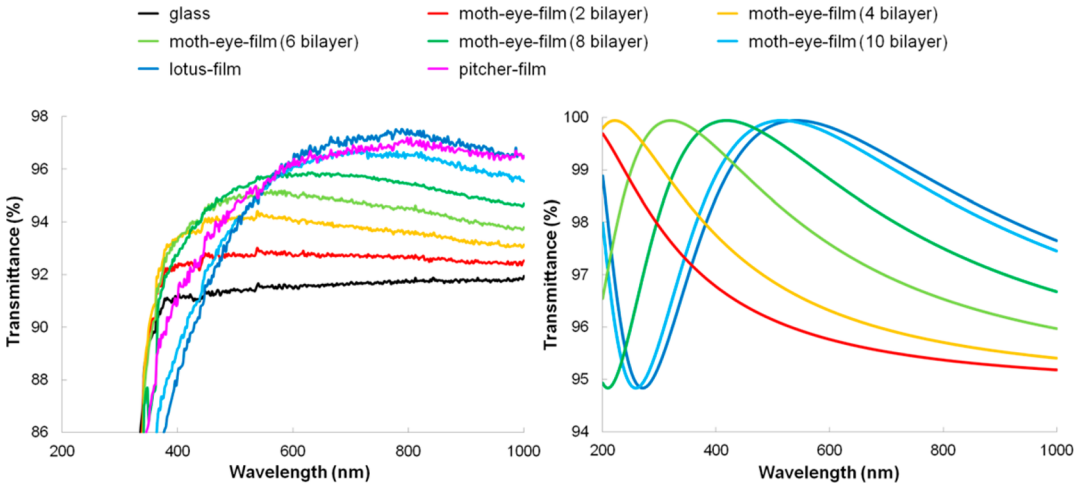

Figure 5. Measured transmittance changes of the films (left) and calculated transmittance changes of each film with the refractive index fixed at 1.23 by optical simulation software (Design, Tecwave), except for the pitcher film (right): transmittance of a glass substrate (black line) and moth-eye films with different numbers of bilayers (two bilayers, red line; four bilayers, yellow line; six bilayers, lime green line; eight bilayers, green line; ten bilayers, aqua line), the lotus film (blue line), and the pitcher film (pink line) on glass substrates in air as the background.

toward the glass substrate. The films were fabricated by stable electrostatic interaction. Therefore, as alternating layers were deposited, a layer with lower refractive index than that of the previous layer was formed. When the refractive index of the interface changes from 1.0 to 1.5, the reflectance is about 4%. The reflectance of each interface is about 0.1−0.2% and the total reflectance is about 0.8% as the refractive index gradually changes by 0.1 toward the glass substrate (Figure 3S, Supporting Information).[53] In this study, each layer was stable because of strong electrostatic interaction, so reflectance can be simply calculated (Figure 3S). Indeed, the moth-eye film (10 bilayers) showed little reflectance compared with the glass substrate under a fluorescent light (Figure 4B).

A single-layer antireflection coating can be made non-reflective only at one wavelength. Assuming a coating thickness a quarter the wavelength in the medium, the reflection can be calculated using the normal incidence reflection coefficients:[53]

$$D = \lambda/4n_1 \tag{4}$$

Therefore, a film with a thickness of D nm shows the highest transmittance at a wavelength of around $4Dn_1$ nm. In this study, each bilayer film shows its highest transmittance at a particular

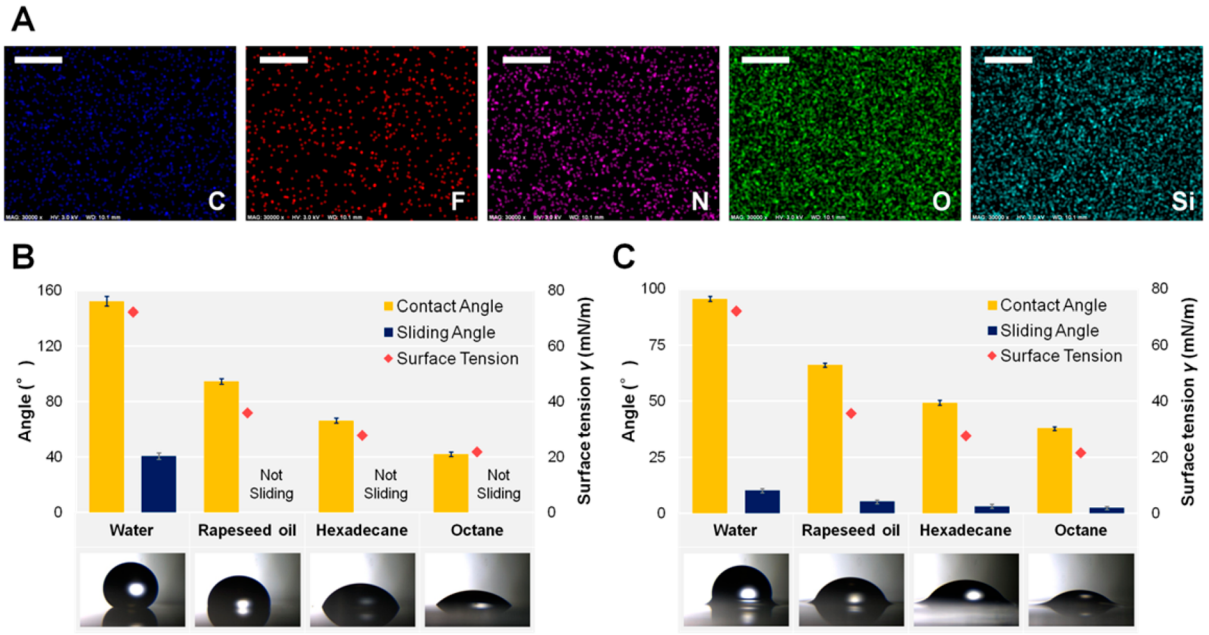

Figure 6. (A) EDX images of the lotus film. All scale bars are 1 μm. Below the EDX images, the graphs demonstrate the contact angle (yellow bars), sliding angle (blue bars), and surface tension (red tilted squares) of water, rapeseed oil, hexadecane, and octane on the (B) lotus film and (C) pitcher film with corresponding photographic images of each liquid drop on the films shown below.

wavelength according to an optical simulation (Figure 5). Also, single-layer antireflection coatings are generally produced for a midrange wavelength such as 550 nm. In the case of $n_1 = 1.23$, $D \cong 112$ nm. The absorbance of the silica and glass substrate increases for incoming light with a wavelength lower than around 350 nm. Therefore, even if the refractive index was ideal, such as for the six-bilayer moth-eye film, the highest transmittance of this film was lower than that of the equivalent eight- and ten-bilayer films, because the wavelength that shows the maximum transmittance is equal to or lower than the absorption wavelength of SiO_2 and the substrate. In the eight-bilayer moth-eye film, the wavelength that has the maximum theoretical transmittance is near the absorption wavelength of silica and the substrate, so incoming light was absorbed. Additionally, scattering near the wavelength with the highest transmittance was increased by Rayleigh scattering because the RMS of this film was larger than 1/10 of the wavelength. As a result, the transmittance of the eight-bilayer moth-eye film decreased. In the 10-bilayer moth-eye film, scattering of short-wavelength light increased because it had a larger surface roughness than the other films. However, the 10-bilayer film was near the ideal thickness (112 nm), and the incoming light was not absorbed near the wavelength with the highest transmittance by silica and the substrate. Also, though an increase of the surface roughness causes scattering to increase, in the case of antireflection films formed by LbL assembly, the thicker the film, the more gradual the change of refractive index. The films show an increasing resemblance to the actual moth-eye structure as the number of bilayers increases.

The reason why the transmittance of all films was lower than the theoretical value and did not reach 100% was because there was a refractive index distribution in the films. In a homogeneous medium, all scattering intensity that is not parallel to the incident beam is annihilated by destructive interference. To observe the scattering intensity, the density and refractive index of the medium need to be inhomogeneous. These inhomogeneities can occur as fluctuations. The scattering intensity is high when the fluctuations are large. According to the above-mentioned theory, it is necessary to increase the air space in a film to decrease its refractive index. However, this causes refractive index distribution and bias in the films. As a result, incoming light was scattered, and the transmittance of the films did not achieve the ideal value. In particular, scattering of short-wavelength light readily occurred for this reason.

Transparent Superhydrophobic Film (Lotus Film). Next a transparent superhydrophobic film (lotus film) was fabricated by functionalizing a 10-bilayer moth-eye film, which had the highest transmittance and surface roughness and lowest refractive index among the moth-eye films. The thickness and refractive index of the lotus film increased compared with those of the moth-eye film because of thermally expanded film components, especially CHINFs, after gas-phase treatment (Figure 3). The refractive index was ideal on a glass substrate for a reflectance of zero, and the film thickness was also almost ideal (112 nm). As the film thickness increased, the surface roughness increased slightly (Figure 4). The highest transmittance of the lotus film was 97.5% at 788 nm (Figure 5).

EDX images of the lotus film indicate that the film modified by (fluoroalkyl)silane contained F, which caused the surface to have a low energy (Figure 6A). These measurements also confirmed that the films contained CHINFs and SiO_2 because both C and N of CHINFs and Si were observed in the films.

Regarding the surface wettability of the lotus film, its contact angle decreased with the surface tension, and the average water contact angle was 152°, indicating superhydrophobic performance (Figure 6B). Rapeseed oil, hexadecane, and octane did not slide on the lotus film. Superhydrophobic surfaces are generated by an air layer existing between a drop of liquid and rough surface.[21,22] However, it is difficult to form an air layer in the case of a liquid with a low surface tension, because the liquid can move through the relief and porous structure. As a result, rapeseed oil, hexadecane, and octane stuck rather than slid on the lotus film.

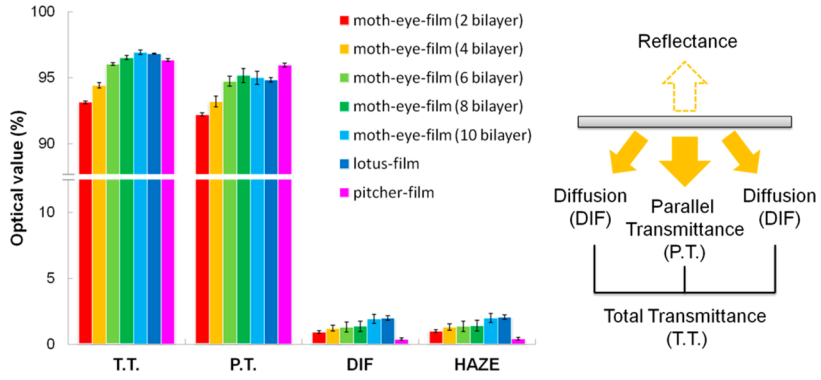

Figure 7. Total transmittance (TT), parallel transmittance (PT), diffusion (DIF), and haze (HAZE) of moth-eye films (two bilayers, red bars; four bilayers, yellow bars; six bilayers, lime green bars; eight bilayers, green bars; ten bilayers, aqua bars), the lotus film (blue bars), and the pitcher film (pink bars). Each optical value is explained on the right. The haze, which describes the amount of light scattering when the light passes through the films, is calculated by dividing DIF by TT.

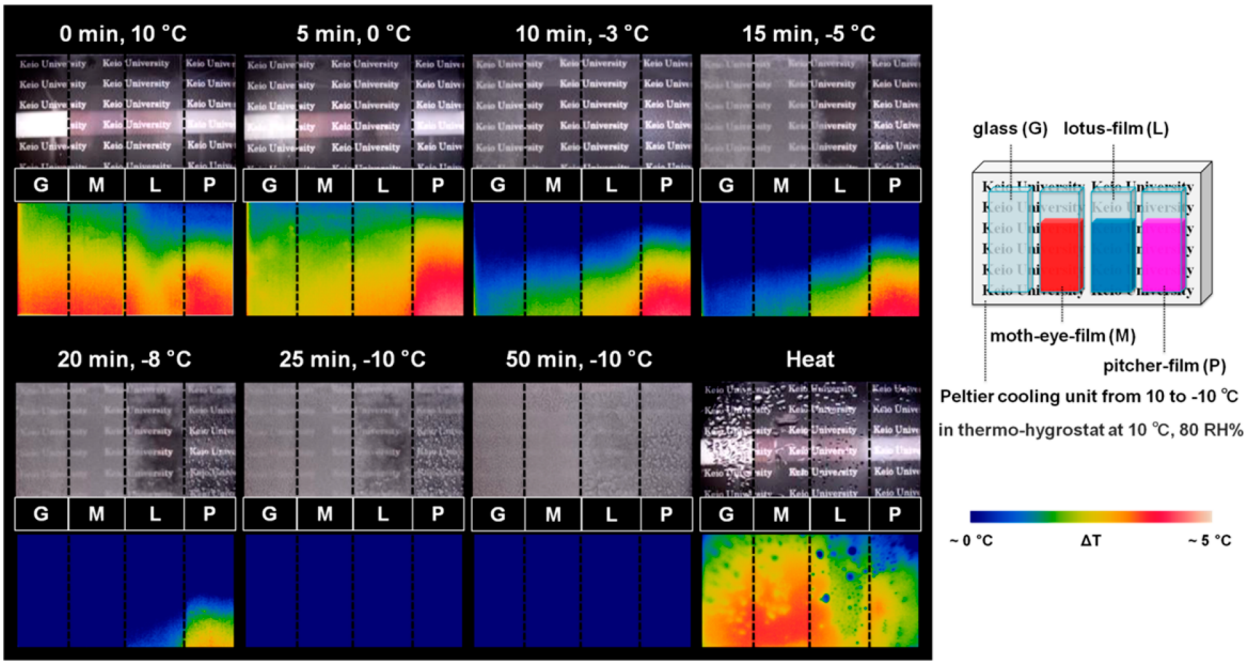

Figure 8. Photo and thermography images of the glass substrate (G), moth-eye film (10-bilayer, M), lotus film (L), and pitcher film (P). Above each image, the elapsed time and temperature since the Peltier cooling unit was turned on are displayed. The temperature was determined by the Peltier unit. The experiment was conducted as shown on the right; that is, the films were placed in a thermohygrostat at 10 °C and 80% RH. The temperature of the Peltier unit was slowly decreased from +10 to −10 °C. The temperature of the Peltier unit was then increased to 30 °C.

The maximum transmittance of the lotus film was higher than that of the moth-eye film (Figure 5), because it had a refractive index of 1.23 (Figure 3). However, the total optical values of visible light of the lotus and moth-eye films (10-bilayer) were almost the same (Figure 7), because of the increase in the surface roughness induced by modification, increasing the Rayleigh scattering.[61] This was confirmed by the decrease of parallel transmission (94.8%) and increase of diffusion (2.05%) of the lotus film compared with the moth-eye film.

Slippery Fluid-Infused Antireflective Film (Pitcher Film). The contact and sliding angles of the pitcher film that was fabricated by dropping a lubricant oil, PFPE, on the lotus film decreased with the surface tension. The sliding angle of water on the pitcher film was 10°, while that of the oil ranged from 2° to 5° (Figure 6C).

The highest transmittance of the pitcher film was 97.2% at 798 nm (Figure 5), and the haze of 0.41% was lower than that of the other films (Figure 7). The haze can be expressed by the following equation:

$$\text{HAZE} = (\text{DIF}/\text{TT}) \times 100 \quad (5)$$

where HAZE, DIF, and TT are the optical values of haze, diffusion, and total transmittance, respectively. Despite possessing total transmittance similar to those of the other films, the parallel transmittance of the pitcher film increased and diffusion decreased, which means light scattering caused by the surface topography and the difference in the refractive index at the solid−gas interface decreased upon the film being covered with lubricant oil. However, the reflectance was higher than that of the other films because of fluctuation in the density of the lubricant oil. In addition, these results indicate that scattering was not caused by the film components, which means

that CHINFs and nanoparticles were sufficiently small compared with the visible wavelength to give at most 0.41% scattering.

Antifrosting Properties. Finally, the antifrosting properties of a glass substrate, moth-eye film (10-bilayer), lotus film, and pitcher film were determined (Figure 8, Supporting Information movie). Before the Peltier cooling unit was turned on, the moth-eye film, lotus film, and pitcher film were antireflective. The lotus film misted over a little because of the attachment of a small nuclear fog on the film 5 min after the Peltier unit was turned on. After 10 min, the parts of the glass substrates without films were covered with fog, which caused inhomogeneous temperature distributions in the same plane. Compared with the glass substrate, the moth-eye film exhibited some antifogging ability.[62] However, the glass substrate and moth-eye film were totally frosted after 15 min. In contrast, frost did not form on the lotus film and pitcher film except for the parts of the substrates without films, which created a temperature difference between the top and bottom. From 15 to 50 min, the lotus film and pitcher film gradually frosted, but they possessed better antifrosting performance compared with the glass substrate and moth-eye film. The temperature on the lotus film decreased more rapidly than that on the pitcher film because the lotus film held fog in its rough surface while fog slipped over the pitcher film until it had low fluidity. Water droplets remained in the specific relief structure of the superhydrophobic surface of the lotus film after heating. In contrast, as the temperature of the Peltier unit increased, dew continued to slide over the pitcher film. Thermography showed that the rate of temperature change on the pitcher film was slower than that on the other films because of the presence of the lubricant oil. Additionally, all of the films maintained their antireflective properties before and after antifrosting testing.

The surface of the pitcher film maintained a relatively small rise in temperature by keeping dew sliding. Once the temperature of the lubricant oil decreased to the point where it was difficult to maintain its fluid surface, frost formation was promoted. Then all surfaces were covered with frost. In contrast, the temperature of the surface increased easily because the water droplets with a high specific heat readily slipped as the temperature of the Peltier unit started to increase.

The above results reveal that slippery fluid-infused films can exhibit antifrosting ability by not only leading to inhibition of fog settlement on the surface, but also suppressing changes of temperature, which was induced by the poor heat transfer of the lubricant.

CONCLUSIONS

In conclusion, antireflective films composed of CHINFs and SiO_2 fabricated by LbL self-assembly exhibited a highest transmittance of 96.7% and lowest refractive index of 1.20 because of their high porosity generated by the nanofibers and nanoparticles. After modification to improve hydrophobic performance, transparent superhydrophobic films with a highest transmittance of 97.5%, antireflective behavior, lowest refractive index of 1.23, which can give a reflectance of zero, and water contact angle of 152° were produced. Dropping lubricant on this film produced a slippery fluid-infused antireflective film with a highest transmittance of 97.2% by decreasing scattering of relief structures and antireflection behavior by gradually changing the refractive index. The transmittance of the latter film is higher than that obtained previously.[23−26,46] The CHINFs and nanoparticles in the films were sufficiently small compared with visible wavelengths of light, and all haze values were less than 2.05%. The use of a low-reflectance film as an underlayer for a lubricant improved the transmittance of the liquid-infused surface. Additionally, these three biomimetic structures reveal that lubricant-infused films can prevent frost formation by keeping fog sliding and resisting thermal changes. Technologically, this research was achieved by a combination of three biomimetic approaches. This approach can contribute to improving various materials and opens up a new pathway to generate highly functionalized materials.

ASSOCIATED CONTENT

Supporting Information

Photographic images and schematic diagrams of films with and without superhydrophobic films as an underlayer for a lubricant, FE-SEM images of moth-eye films on each bilayer, ζ potentials of CHINF solutions at different pH values, schematic diagrams of the refractive index changes on bare glass, the moth-eye structure, and the LbL film, and antifrosting movie. This material is available free of charge via the Internet at http://pubs.acs.org/.

AUTHOR INFORMATION

Corresponding Author

*E-mail: shiratori@appi.keio.ac.jp.

Author Contributions

K.M. conceived, designed, and carried out the experiments, analyzed the data, and wrote the paper. S.N. and K.-H.K. provided experimental support and support in data analysis. S.S. gave scientific advice. S.S. and S.N. commented on the manuscript.

Notes

The authors declare no competing financial interest.

ACKNOWLEDGMENTS

We are deeply grateful to Dr. Kouji Fujimoto and Mr. Naoyuki Yokoi, whose comments and suggestions were innumerably valuable throughout our study. We are indebted to Dr. Yoshio Hotta, whose meticulous comments were an enormous help.

REFERENCES

(1) Lepora, N. F.; Verschure, P.; Prescott, T. J. The State of the Art in Biomimetics. *Bioinspiration Biomimetics* **2013**, *8*, 1.

(2) Bhushan, B. Biomimetics: Lessons from Nature—An Overview. *Philos. Trans. R. Soc. London, Ser. A* **2009**, *367*, 1445−1486.

(3) Sarikaya, M.; Tamerler, C.; Jen, A. K. Y.; Schulten, K.; Baneyx, F. Molecular Biomimetics: Nanotechnology through Biology. *Nat. Mater.* **2003**, *2*, 577−585.

(4) Sun, T.; Feng, L.; Gao, X.; Jiang, L. Bioinspired Surfaces with Special Wettability. *Acc. Chem. Res.* **2005**, *38*, 644−652.

(5) Zhai, L.; Cebeci, F. C.; Cohen, R. E.; Rubner, M. F. Stable Superhydrophobic Coatings from Polyelectrolyte Multilayers. *Nano Lett.* **2004**, *4*, 1349−1353.

(6) Miyauchi, Y.; Ding, B.; Shiratori, S. Fabrication of a Silver-Ragwort-Leaf-like Super-Hydrophobic Micro/Nanoporous Fibrous Mat Surface by Electrospinning. *Nanotechnology* **2006**, *17*, 5151−5156.

(7) Chung, K. K.; Schumacher, J. F.; Sampson, E. M.; Burne, R. A.; Antonelli, P. J.; Brennan, A. B. Impact of Engineered Surface Microtopography on Biofilm Formation of *Staphylococcus aureus*. *Biointerphases* **2007**, *2*, 89−94.

(8) Manabe, K.; Nishizawa, S.; Shiratori, S. Porous Surface Structure Fabricated by Breath Figures that Suppresses *Pseudomonas aeruginosa* Biofilm Formation. *ACS Appl. Mater. Interfaces* **2013**, *5*, 11900−11905.

(9) Huang, Y.-F.; Chattopadhyay, S.; Jen, Y.-J.; Peng, C.-Y.; Liu, T.-A.; Hsu, Y.-K.; Pan, C.-L.; Lo, H.-C.; Hsu, C.-H.; Chang, Y.-H.; Lee, C.-S.; Chen, K.-H.; Chen, L.-C. Improved Broadband and Quasi-Omnidirectional Anti-Reflection Properties with Biomimetic Silicon Nanostructures. *Nat. Nanotechnol.* **2007**, *2*, 770−774.
(10) Forberich, K.; Dennler, G.; Scharber, M. C.; Hingerl, K.; Fromherz, T.; Brabec, C. J. Performance Improvement of Organic Solar Cells with Moth Eye Anti-Reflection Coating. *Thin Solid Films* **2008**, *516*, 7167−7170.
(11) Hiller, J. A.; Mendelsohn, J. D.; Rubner, M. F. Reversibly Erasable Nanoporous Anti-Reflection Coatings from Polyelectrolyte Multilayers. *Nat. Mater.* **2002**, *1*, 59−63.
(12) Parker, A. R.; Lawrence, C. R. Water Capture by a Desert Beetle. *Nature* **2001**, *414*, 33−34.
(13) Zhai, L.; Berg, M. C.; Cebeci, F. C.; Kim, Y.; Milwid, J. M.; Rubner, M. F.; Cohen, R. E. Patterned Superhydrophobic Surfaces: Toward a Synthetic Mimic of the Namib Desert Beetle. *Nano Lett.* **2006**, *6*, 1213−1217.
(14) Feng, X. J.; Jiang, L. Design and Creation of Superwetting/Antiwetting Surfaces. *Adv. Mater.* **2006**, *18*, 3063−3078.
(15) Autumn, K.; Liang, Y. A.; Hsieh, S. T.; Zesch, W.; Chan, W. P.; Kenny, T. W.; Fearing, R.; Full, R. J. Adhesive Force of a Single Gecko Foot-Hair. *Nature* **2000**, *405*, 681−685.
(16) Ma, M.; Hill, R. M. Superhydrophobic Surfaces. *Curr. Opin. Colloid Interface Sci.* **2006**, *11*, 193−202.
(17) Nishizawa, S.; Shiratori, S. Fabrication of Semi-Transparent Superoleophobic Thin Film by Nanoparticle-Based Nano−Micro-structures on See-Through Fabrics. *J. Mater. Sci.* **2013**, *48*, 6613−6618.
(18) Nishizawa, S.; Shiratori, S. Water-Based Preparation of Highly Oleophobic Thin Films through Aggregation of Nanoparticles Using Layer-by-Layer Treatment. *Appl. Surf. Sci.* **2012**, *263*, 8−13.
(19) Wang, F. J.; Lei, S.; Ou, J. F.; Xue, M. S.; Li, W. Superhydrophobic Surfaces with Excellent Mechanical Durability and Easy Repairability. *Appl. Surf. Sci.* **2013**, *276*, 397−400.
(20) Bravo, J.; Zhai, L.; Wu, Z.; Cohen, R. E.; Rubner, M. F. Transparent Superhydrophobic Films Based on Silica Nanoparticles. *Langmuir* **2007**, *23*, 7293−7298.
(21) Gao, X.; Yan, X.; Yao, X.; Xu, L.; Zhang, K.; Zhang, J.; Yang, B.; Jiang, L. The Dry-Style Antifogging Properties of Mosquito Compound Eyes and Artificial Analogues Prepared by Soft Lithography. *Adv. Mater.* **2007**, *19*, 2213−2217.
(22) Kim, P.; Wong, T. S.; Alvarenga, J.; Kreder, M. J.; Adorno-Martinez, W. E.; Aizenberg, J. Liquid-Infused Nanostructured Surfaces with Extreme Anti-Ice and Anti-Frost Performance. *ACS Nano* **2012**, *6*, 6569−6577.
(23) Wong, T. S.; Kang, S. H.; Tang, S. K.; Smythe, E. J.; Hatton, B. D.; Grinthal, A.; Aizenberg, J. Bioinspired Self-Repairing Slippery Surfaces with Pressure-Stable Omniphobicity. *Nature* **2011**, *477*, 443−447.
(24) Ma, W.; Higaki, Y.; Otsuka, H.; Takahara, A. Perfluoropolyether-Infused Nano-Texture: A Versatile Approach to Omniphobic Coatings with Low Hysteresis and High Transparency. *Chem. Commun.* **2013**, *49*, 597−599.
(25) Kim, P.; Kreder, M. J.; Alvarenga, J.; Aizenberg, J. Hierarchical or Not? Effect of the Length Scale and Hierarchy of the Surface Roughness on Omniphobicity of Lubricant-Infused Substrates. *Nano Lett.* **2013**, *13*, 1793−1799.
(26) Vogel, N.; Belisle, R. A.; Hatton, B.; Wong, T. S.; Aizenberg, J. Transparency and Damage Tolerance of Patternable Omniphobic Lubricated Surfaces Based on Inverse Colloidal Monolayers. *Nat. Commun.* **2013**, *4*, 2176.
(27) Wilson, P. W.; Lu, W.; Xu, H.; Kim, P.; Kreder, M. J.; Alvarenga, J.; Aizenberg, J. Inhibition of Ice Nucleation by Slippery Liquid-Infused Porous Surfaces (SLIPS). *Phys. Chem. Chem. Phys.* **2013**, *15*, 581−585.
(28) Smith, J. D.; Dhiman, R.; Anand, S.; Reza-Garduno, E.; Cohen, R. E.; McKinley, G. H.; Varanasi, K. K. Droplet Mobility on Lubricant-Impregnated Surfaces. *Soft Matter* **2013**, *9*, 1772−1780.
(29) Yao, X.; Hu, Y.; Grinthal, A.; Wong, T. S.; Mahadevan, L.; Aizenberg, J. Adaptive Fluid-Infused Porous Films with Tunable Transparency and Wettability. *Nat. Mater.* **2013**, *12*, 529−534.
(30) Clapham, P. B.; Hutley, M. C. Reduction of Lens Reflexion by the "Moth Eye" Principle. *Nature* **1973**, *244*, 281−282.
(31) Koo, H. Y.; Yi, D. K.; Yoo, S. J.; Kim, D. Y. A Snowman-like Array of Colloidal Dimers for Antireflecting Surfaces. *Adv. Mater.* **2004**, *16*, 274−277.
(32) Lvov, Y.; Decher, G.; Moehwald, H. Assembly, Structural Characterization, and Thermal Behavior of Layer-by-Layer Deposited Ultrathin Films of Poly(vinyl sulfate) and Poly(allylamine). *Langmuir* **1993**, *9*, 481−486.
(33) Shiratori, S. S.; Rubner, M. F. pH-Dependent Thickness Behavior of Sequentially Adsorbed Layers of Weak Polyelectrolytes. *Macromolecules* **2000**, *33*, 4213−4219.
(34) Matsuda, M.; Shiratori, S. Correlation of Antithrombogenicity and Heat Treatment for Layer-by-Layer Self-Assembled Polyelectrolyte Films. *Langmuir* **2011**, *27*, 4271−4277.
(35) Lvov, Y.; Ariga, K.; Ichinose, I.; Kunitake, T. Assembly of Multicomponent Protein Films by Means of Electrostatic Layer-by-Layer Adsorption. *J. Am. Chem. Soc.* **1995**, *117*, 6117−6123.
(36) Lu, Y.; Choi, Y. J.; Lim, H. S.; Kwak, D.; Shim, C.; Lee, S. G.; Cho, K. pH-Induced Antireflection Coatings Derived from Hydrogen-Bonding-Directed Multilayer Films. *Langmuir* **2010**, *26*, 17749−17755.
(37) Zhang, L.; Sun, J. Layer-by-Layer Codeposition of Polyelectrolyte Complexes and Free Polyelectrolytes for the Fabrication of Polymeric Coatings. *Macromolecules* **2010**, *43*, 2413−2420.
(38) Yuan, W.; Li, C. M. Exponentially Growing Layer-by-Layer Assembly To Fabricate pH-Responsive Hierarchical Nanoporous Polymeric Film and Its Superior Controlled Release Performance. *Chem. Commun.* **2010**, *46*, 9161−9163.
(39) Nogueira, G. M.; Swiston, A. J.; Beppu, M. M.; Rubner, M. F. Layer-by-Layer Deposited Chitosan/Silk Fibroin Thin Films with Anisotropic Nanofiber Alignment. *Langmuir* **2010**, *26*, 8953−8958.
(40) Shimomura, H.; Gemici, Z.; Cohen, R. E.; Rubner, M. F. Layer-by-Layer-Assembled High-Performance Broadband Antireflection Coatings. *ACS Appl. Mater. Interfaces* **2010**, *2*, 813−820.
(41) Qi, Z. D.; Saito, T.; Fan, Y.; Isogai, A. Multifunctional Coating Films by Layer-by-Layer Deposition of Cellulose and Chitin Nanofibrils. *Biomacromolecules* **2012**, *13*, 553−558.
(42) Decher, G.; Schlenoff, J. B. *Multilayer Thin Films: Sequential Assembly of Nanocomposite Materials*; Wiley-VCH Verlag GmbH & Co.: Weinheim, Germany, 2003.
(43) Kim, J. H.; Fujita, S.; Shiratori, S. Design of a Thin Film for Optical Applications, Consisting of High and Low Refractive Index Multilayers, Fabricated by a Layer-by-Layer Self-Assembly Method. *Colloids Surf., A* **2006**, *284*, 290−294.
(44) Zhao, N.; Shi, F.; Wang, Z.; Zhang, X. Combining Layer-by-Layer Assembly with Electrodeposition of Silver Aggregates for Fabricating Superhydrophobic Surfaces. *Langmuir* **2005**, *21*, 4713−4716.
(45) Huang, X.; Chrisman, J. D.; Zacharia, N. S. Omniphobic Slippery Coatings Based on Lubricant-Infused Porous Polyelectrolyte Multilayers. *ACS Macro Lett.* **2013**, *2*, 826−829.
(46) Okada, I.; Shiratori, S. High-Transparency, Self-Standable Gel-SLIPS Fabricated by a Facile Nanoscale Phase Separation. *ACS Appl. Mater. Interfaces* **2014**, *6*, 1502−1508.
(47) Li, Y.; Chen, S.; Wu, M.; Sun, J. Polyelectrolyte Multilayers Impart Healability to Highly Electrically Conductive Films. *Adv. Mater.* **2012**, *24*, 4578−4582.
(48) Ma, Y.; Zhang, Y.; Wu, B.; Sun, W.; Li, Z.; Sun, J. Polyelectrolyte Multilayer Films for Building Energetic Walking Devices. *Angew. Chem., Int. Ed.* **2011**, *123*, 6378−6381.
(49) Ma, Y.; Sun, J. Humido- and Thermo-Responsive Free-Standing Films Mimicking the Petals of the Morning Glory Flower. *Chem. Mater.* **2009**, *21*, 898−902.
(50) Ifuku, S.; Nogi, M.; Abe, K.; Yoshioka, M.; Morimoto, M.; Saimoto, H.; Yano, H. Preparation of Chitin Nanofibers with a

Uniform Width as A-Chitin from Crab Shells. *Biomacromolecules* **2009**, *10*, 1584−1588.
(51) Gopalan Nair, K.; Dufresne, A. Crab Shell Chitin Whisker Reinforced Natural Rubber Nanocomposites. 1. Processing and Swelling Behavior. *Biomacromolecules* **2003**, *4*, 657−665.
(52) Fan, Y.; Saito, T.; Isogai, A. Individual Chitin Nano-Whiskers Prepared from Partially Deacetylated A-Chitin by Fibril Surface Cationization. *Carbohydr. Polym.* **2010**, *79*, 1046−1051.
(53) MacLeod, H. A. *Thin-film Optical Filters*, 2nd ed.; Macmillan: New York, 1986.
(54) Tan, W. S.; Du, Y.; Luna, L. E.; Khitass, Y.; Cohen, R. E.; Rubner, M. F. Templated Nanopores for Robust Functional Surface Porosity in Poly(methyl methacrylate). *Langmuir* **2012**, *28*, 13496−13502.
(55) Whyman, G.; Bormashenko, E. How To Make the Cassie Wetting State Stable? *Langmuir* **2011**, *27*, 8171−8176.
(56) Eastman, J.; Bausmeister, P. The Microstructure of Polished Optical Surfaces. *Opt. Commun.* **1974**, *12*, 418−420.
(57) Arnon, O. Loss Mechanisms in Dielectric Optical Interference Devices. *Appl. Opt.* **1977**, *16*, 2147−2151.
(58) Bennett, H.; Porteus, J. O. Relation between Surface Roughness and Specular Reflectance at Normal Incidence. *J. Opt. Soc. Am.* **1961**, *51*, 123−129.
(59) Carniglia, C. K. Scalar Scattering Theory for Multilayer Optical Coatings. *Opt. Eng.* **1979**, *18*, 104−115.
(60) Roos, A.; Rönnow, D. Diffuse Reflectance and Transmittance Spectra of an Interference Layer: 1. Model Formulation and Properties. *Appl. Opt.* **1994**, *33*, 7908−7917.
(61) Kelly, K. L.; Coronado, E.; Zhao, L. L.; Schatz, G. C. The Optical Properties of Metal Nanoparticles: The Influence of Size, Shape, and Dielectric Environment. *J. Phys. Chem. B* **2003**, *107*, 668−677.
(62) Cebeci, F. Ç.; Wu, Z.; Zhai, L.; Cohen, R. E.; Rubner, M. F. Nanoporosity-Driven Superhydrophilicity: A Means To Create Multifunctional Antifogging Coatings. *Langmuir* **2006**, *22*, 2856−2862.